Hindawi
Geofluids
Volume 2022, Article ID 8130349, 15 pages
https://doi.org/10.1155/2022/8130349

Research Article

Main Factors of Mesozoic Tectonic Deformation in the Erlian Basin, Inner Mongolia, China: Insights from Physical Modelling

Yue Zhao,[1] Qiang Xu,[1] Yongchen Li,[2] Xiujia Bai,[1] Rong Ding,[2] Jianxin Wang,[3] and Tao Hou[4]

[1]*General Prospecting Institute of China National Administration of Coal Geology, Beijing 100039, China*
[2]*PetroChina Coalbed Methane Company Limited 100028, China*
[3]*China National Offshore Oil Corporation Research Institute, Beijing 100028, China*
[4]*Petrochina Huabei Oilfield Company, Renqiu 062550, China*

Correspondence should be addressed to Qiang Xu; 454123526@qq.com

Received 14 February 2022; Accepted 7 April 2022; Published 4 May 2022

Academic Editor: Yanjun Meng

Erlian Basin is a Mesozoic oil and gas-bearing basin in northeast of China. The extension rate, extension direction, and stratum thickness of this rift basin have a clear control on its shape and extension. In this study, we design three sandbox models of the Erlian Basin to represent the effects of changing these three factors. The extension rate controls the timing of secondary fault formation inside the rift basin; a high extension rate promotes faster deformation inside the rift. The extension direction controls the strike of the fault inside the rift; a greater angle between the extension direction and the normal direction of the strike of the rift favors rapid evolution of internal secondary faults. The stratum thickness represents the control of sedimentation on the rift basin; the thinner the brittle layer, the wider the rift. The simulation results also show that the extension direction is the major factor controlling tectonic deformation in the basin. Stratum thickness and extension rate are secondary controlling factors. Additionally, according to geometric and kinematic similarities between typical Mesozoic rift basins in eastern and adjacent areas of China, we suggest that southeastward extension is a possible kinematic mechanism for basin formation.

1. Introduction

Erlian Basin is a Mesozoic oil- and gas-bearing basin in northeast China (Figure 1). There are significant geometric and kinematic similarities between Erlian Basin and other Mesozoic rift basins in eastern China [1–8]. For example, the structural style of fault depression in both Erlian Basin and peripheral Mesozoic rift basins such as Hailar Basin and Yin'e Basin predominantly includes a long, narrow half graben, a graben, and a composite structure combining the two [1]. The evolutionary features of the study area can be divided into two stages of tectonic deformation: Mesozoic early continental and late depression [9, 10]. Previous research has involved long-term oil and gas exploration of the basin ([11]) and indicates that tectonic deformation plays an important role in controlling the distribution of oil and gas resources [5]. Consequently, there is an in-depth understanding of the distribution of early Cretaceous oil-bearing strata and the structural characteristics formed by continental rifting in this basin. According to previous research on the factors controlling basin deformation, four different models have been proposed: (1) The formation and distribution of rifting in the Erlian Basin were controlled by the pre-Mesozoic basement structure ([12, 13]). (2) The preexisting basal fault network, the tectonic stress field during the rifting period, and other factors at depth all controlled the formation and distribution of the rift basin [1]. (3) Five large-scale, long-active, and deep faults oriented EWW and NE in the basin basement controlled the tectonic evolution of the basin in different periods [14]. (4) The basement properties and preexisting structure of the basin controlled the structural pattern of the basin [5, 15, 16]. Thus,

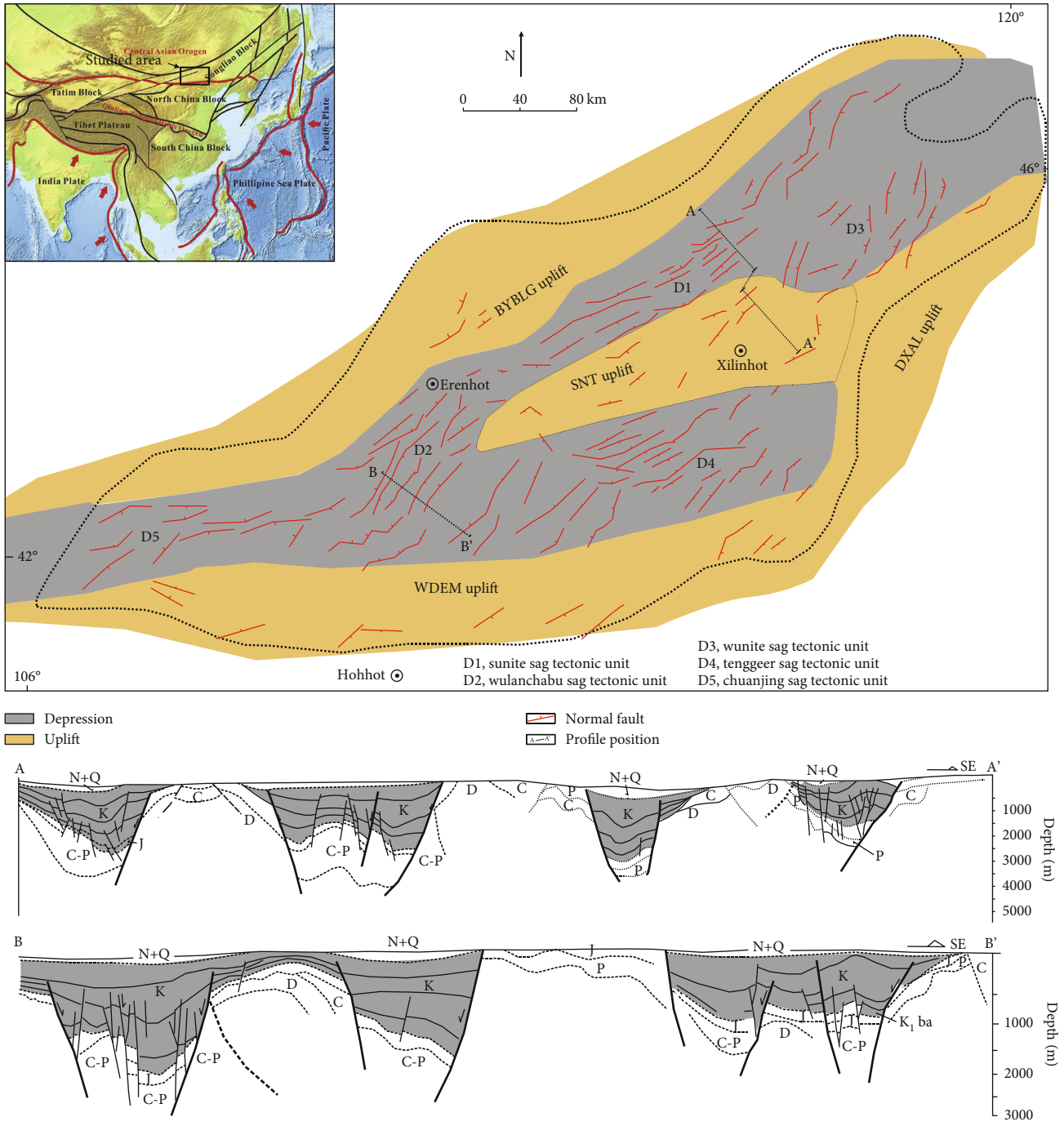

Figure 1: Distribution of tectonic units, major faults, and typical sections of faulted-sag basins in Erlian Basin interpreted from seismic data (revised after [16]).

the factors controlling Mesozoic tectonic deformation in the Erlian Basin remain controversial. Specifically, there is a lack of physical models that simulate deformation mechanisms, particularly the influence and control of pre-Mesozoic basement properties on deformation.

Deformation analysis of rifting and extension in basins has shown that physical simulations are an effective way to explore the mechanisms of tectonic formation; they can replicate the tectonic deformation and effectively verify the relevant formation mechanisms and evolution processes. Physical modelling has been widely used for rift and extensional structures and provides many new insights for understanding the tectonic deformation mechanism of rift basins [17, 18]; for example, experiments have shown that rift basin fault strike and combination is related to the extension direction [19–23], boundary geometry [24–26], preexisting structure [27–29], and basement properties [28].

According to the structural characteristics of a seismic section and the distribution characteristics of the planar fault system in the study area, combined with previous geological

analyses, we designed an experimental sandbox model that could control the extension rate, stratum thickness, and extension direction of the basin. The model was used to determine the major factors controlling tectonic deformation in the Erlian Basin, and our experimental results were compared with the present structural features. We then proposed a kinematic mechanism for formation of Erlian Basin and other basins with similar tectonic properties in northeast China.

2. Geological Background

Erlian Basin is generally oriented NNE; it has a wide central area, is narrow in the NE and NW, and has an elliptical shape. The tectonic units consist of five depressions: Sunite Sag, Wulanchabu Sag, Wunite Sag, Tenggeer Sag, and Chuanjing Sag, and three areas of uplift: the BYBLG uplift, SNT uplift, and WDEM uplift (Figure 1). The structural pattern is complex and exhibits different fault strikes. There are a series of three-level structural units inside the depressions and uplifted areas known as sunken areas and bulges. The master fault strike of Sunite Sag and Wulanchabu Sag in the central basin is NE50°–70°. The internal secondary fault depression of the central rift zone in Sunite-Wulanchabu is dominated in tandem and oblique structures and is characterized by a deep and narrow graben and a half graben. Multiple faulted depressions form a narrow, long, and positive fault depression zone, whose strike is essentially consistent with the extension direction of the depression. The strike of the master fault between Chuanjing Sag in the west and Tenggeer Sag in the south is EN50°–70°, whereas that of Wunite Sag in the east is NE15°–451. The internal secondary fault depressions in the rift zone around basin are dominated by oblique structures and are characterized by a shallow and wide graben and a half graben. Multiple fault depression oblique rows form a short, wide, and oblique fault depression zone, whose strike is oblique to the extension direction of the depression [16, 30]. This type of fault depression in the Erlian Basin is widespread in the rift basins of northeastern China, such as Hailar Basin and Yin'e Basin in the west of the Greater Khingan Mountains, which have a similar distribution direction and shape and combine to form the Mongolian fault basin system [10, 31].

The Erlian Basin is divided into three sets of construction. Internally, the pre-Mesozoic basement includes the Atrial crystalline metamorphic rock, Proterozoic era, and Paleozoic sedimentary rocks. Mesozoic Strata is the main body of the basins, including the Jurassic, the Lower Cretaceous, and a small amount of Upper Cretaceous, missing Triassic. Among them, the whole basin of the Jurassic is widely distributed, mainly in volcanic debris, volcanic rock, etc., and the thickness of the formation is relatively stable. The Lower Cretaceous is mainly filled with a series of debris rock layers, and the formation thickness is obviously subject to fault control. The Upper Cretaceous is only sporadic in partial depression; the Neogene and Quaternary are mainly distributed in the depression zone.

The basement of the Erlian Basin belongs to the Mongolian orogenic belt and has undergone multiple stages of tectonic evolution, including the Caledonian, Hercynian, Indosinian, and early Yanshanian periods. The basement structure is characterized by nonuniformity and composed of three anticlinorium and two synclinorium [32], which constitute a positive and negative tectonic pattern, as well as a number of large-scale faults oriented NNE and NE. Among them, the NE-NEE Erlian-Hegenshan fault and deep, near EW Ondor Sum-Xar Moron fault form two important structural boundaries. They divide the basement into three regions with significantly different tectonic directions and crustal structure properties, revealing the complex structural features of the strong deformation zone surrounding the weakly deformed block body. The anticlinorium uplift zone belongs to the weak deformation zone of the basement and forms the uplift zones of the basin. The synclinorium or fault zone belongs to the strong deformation zone of the basement, which mainly controls the development of basin depressions. Sunite Sag and Wulanchabu Sag in the middle of the basin are superimposed on the Dong Ujimqin-Erlian curved fold belt, which strikes from NE to NEE and protrudes southward. The strike of the master fault in the rift is essentially the same as that of the basement structure. Sunite Sag in the eastern margin of the basin is superimposed on the NEE-striking Erlian-Hegenshan Deep Fault Zone, whereas Chuanjing-Tenggeer Sag is superimposed on the EW-striking Ondor Sum-Xar Moron Deep Fault Zone, and on both sides of the fold belt, the strike of the master fault in the rift is oblique to the strike of the basement structure [16].

Some seismic sections in the Erlian Basin exhibit deformation characteristics of rapid Mesozoic rifting and slow late settlement (Figure 1), as well as strongly continuous fault activity. Early Cretaceous fault activity was strong, and fault displacement was large before weakening in the late stage. The structure pattern of the central positive rift zone is half-graben in tandem and codirectional composite structure. The master fault has a steep dip angle, and the resulting fault depression is narrow and long. The structural pattern of the peripheral oblique rift zone is half-graben in tandem and oblique arrangement. In the shallow layer, the fault is mainly characterized as a high-angle normal fault, with a dip angle up to 80°, a large fault displacement, a deep part that gradually becomes shovel type, and a resulting fault depression that is shallow and wide (Figure 1 A-A' and B-B').

3. Model Design

All the models in this study used a 60 cm × 45 cm sandbox (Figure 2). The models are driven by a motor to pull one side of the movable baffle; as the rubber at the bottom is stretched, the upper sand layer gradually produces normal faults and different types of rift. The model surface was photographed regularly using a computer-controlled camera. All experiments were repeated, revealing reproducible results. After each experiment, a layer of white quartz sand was spread evenly on the surface of the model to prevent deformation of the model surface. After spraying with water mist, the model was sliced at equidistant intervals to observe the internal deformation. Only one variable was changed in

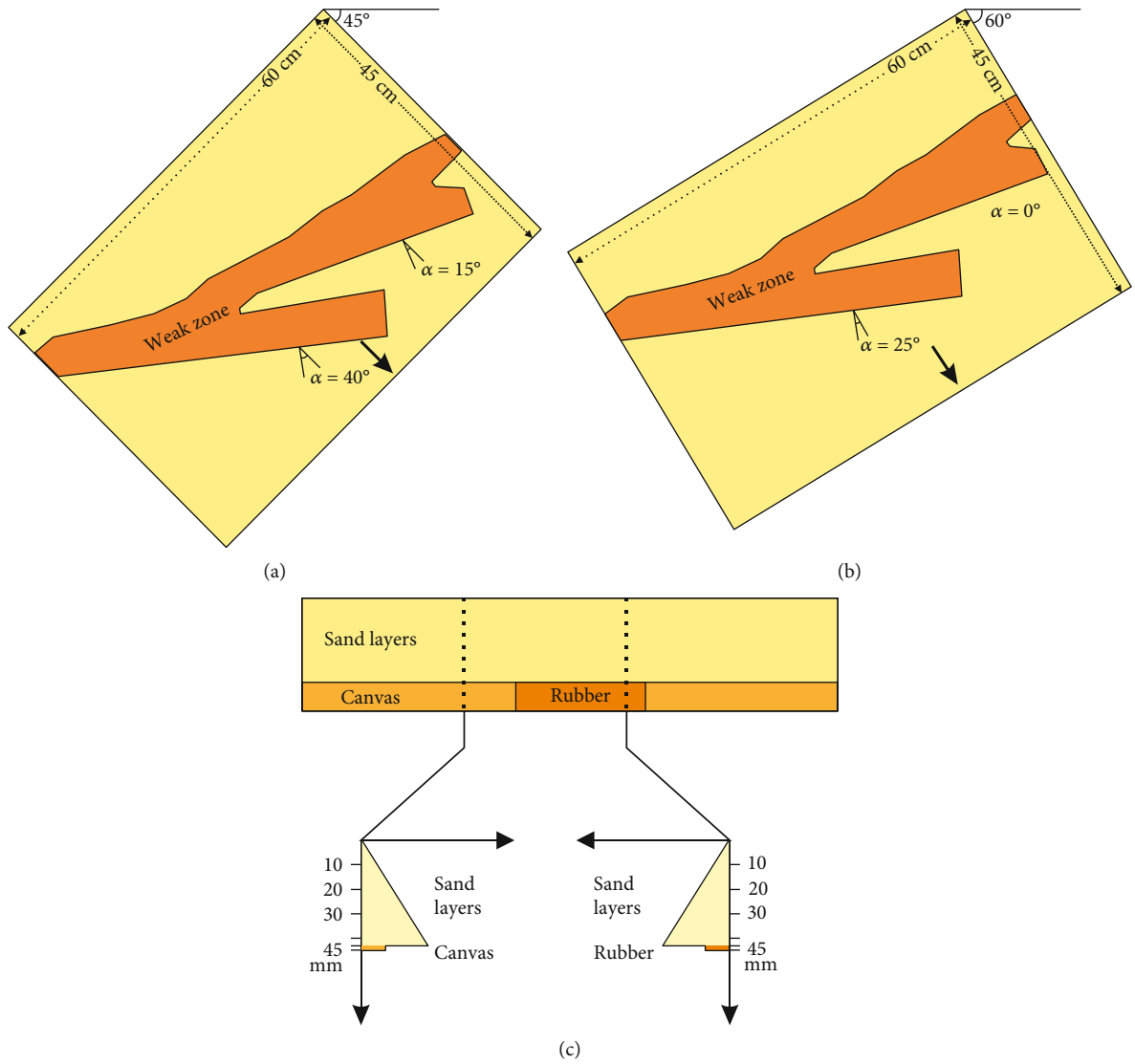

Figure 2: Schematic diagram of the experimental model. (a) Plan view of the extension direction oriented N315°E–N135°E, (b) plan view of the extension direction oriented N330°E–N150°E, and (c) cross-sectional view.

each model to examine the effect of different factors on tectonic deformation. The experimental design was simplified to reduce the impacts of minor factors. The sandbox experiments were carried out in the State Key Laboratory of Oil and Gas Resources and Exploration, China University of Petroleum (Beijing).

3.1. Experimental Setup. All models were 60 cm long and 45 mm wide. The shape of the base retractable eraser was similar to "Y"(Figure 2(a)); this design not only considers the actual Paleozoic basement shape of the Erlian Basin, but also the influence of different oblique rifting directions on tectonic deformation. Except for model 3, all models were 42 mm thick, in which the overlying sand layer was 40 mm and the base retractable rubber and nonstretchable canvas were 2 mm (Figure 2). The initial thickness of the overlying sand layer on model 3 was 25 mm, and a 5 mm sand layer was added for extensions of 20 mm, 40 mm, and 60 mm. The final thickness of the sand layer was therefore 40 mm, like the other models. In order to study the influence of syn-deposition and the thickness of the brittle layer (equivalent to changing the strength of the brittle layer) on tectonic deformation (similar to [33]) (Figure 2(c)), the final extension of all models was 80 mm (Table 1).

This series of models was designed to investigate the effect of stratum thickness, extension rate, and extension direction. Changing the extension direction is equivalent to changing the inclination angle of extension (defined as the angle between the extension direction and the normal direction of the rift) during the rifting process [23, 27, 33]. Model 1 had an extension rate and direction of 6.67×10^{-3} m/s and N315°E–N135°E, respectively. In model 2, the extension rate was changed to 3.35×10^{-2} m/s. In model 4, the extension direction was changed to N330°E–N150°E, which corresponds to a change in the extension inclination angle of $\alpha = 0°$, 25° compared with model 1 (extension angle $\alpha = 15°$, 40°).

Table 1: Parameter table of each sand box simulation experiment model.

Mode	Experimental series	Velocity of extension (mm/min)	Thickness of basement layers (mm)	Thickness of brittle layers (mm)	Extension direction	Syndeposition
1	Reference model	0.4	0.2	4.3	N315°E-N135°E	-
2	Variable extension velocity	2.0	0.2	4.3	N330°E-N150°E	-
3	Syndeposition	0.4	0.2	2.5	N315°E-N135°E°	+
4	Variable extension direction	0.4	0.2	4.3	N315°E-N135°E	-

Table 2: Material parameters of physical simulation experiments.

	Density (g/cm^3)	Particle size (mm)	Internal friction angle (°)	Kinetic friction coefficient	Static friction coefficient	Cohesion (Pa)
Quartz sand	1.43	0.25–0.3	30-31	0.65	0.59	80

3.2. Material Properties. We employed loosely dried quartz sand, which follows the Mohr-coulomb yielding criteria with a particle size of 0.25–0.3 mm, a density of 1.43 g/cm^3, an internal friction angle of 30–31°, a kinetic friction coefficient of 0.65, and a cohesion force close to 80 Pa (Table 2). It is an ideal analog material for simulating shallow structural deformation of the crust [34]. Rubber is widely used in experiments simulating the extensional structure of the rift basin due to its flexible elasticity [29, 35, 36]. This experiment employed the quasi-kinematic retractable eraser to simulate the highly ductile weak basement zone [36]. This weak deformation area was overlain with nonstretchable canvas to transfer the displacement.

3.3. Scaling. The model size ratio is 1×10^{-5}, as 1 cm in the model represents 1 km in reality; thus, the standard model simulates a brittle layer 4 km thick and 60 km long (Table 2). Values for the density, angle of internal friction, and cohesive force of brittle material of the geologic entity are derived from Zhou et al. [37]. The cohesive force of the brittle material in the model is 80 Pa [38], giving a cohesive force ratio of 2×10^{-6} (Table 3).

We apply standard formulas to scale the proportions of our model and actual geologic entity. The brittle sand follows the Mohr-Coulomb yielding criteria, and the stress ratio ($\sigma*$, constant: $\sigma* = \sigma_m/\sigma_n$, subscripts m and n, respectively, represent the model and geologic entity) is as follows [39]:

$$\sigma^* = \rho^* \times h^* \times g^*. \quad (1)$$

The density ratio ($\rho*$) is $\rho_m = 1430\ kg/m^3$ and $\rho_n = 2400\ kg/m^3$. The length ratio ($h*$) is $h_m = 4 \times 10^{-2}$ m and $h_n = 4 \times 10^3$ m. The gravity ratio ($g*$) is $g_m = g_n = 9.81\ m/s^2$. The stress ratio of the model brittle layer is 3×10^{-6}. The above proportions have the same order of magnitude, which indicates that our model satisfies the kinetic similarity criterion [40].

We also determined the ratio, R_s, between the gravity and cohesion force of the brittle region to ensure kinetic similarity between our experiments and the geologic entity [41]:

$$R_S = \frac{\text{gravity}}{\text{cohesion}} = \frac{\rho.g.h}{c}. \quad (2)$$

Table 3: Scaling of models and geologic entity.

Parameter	Model	Nature	Model/nature ratio (*)
Density, ρ (g/cm^3)	1.43	2.40	0.60
Internal friction angle, u	0.65	2.20	0.43
Cohesion, c (Pa)	80	7×10^7	1.14×10^{-6}
Gravity, g (m/s^2)	9.81	9.81	1.00
Length, l (m)	0.01	1000	1.00×10^{-5}
Stress, σ (Pa)	561	9.42×10^7	3.00×10^{-6}
R_s	7.01	2.35	/

The R_s values are 7.01 and 2.35 for the model and geologic entity, respectively ($c_{\text{geologic entity}} = 6 \times 10^7$, according to [42]).

4. Results

4.1. Reference Model (Model 1). The tectonic deformation evolution process of model 1 is shown in Figure 3 (extension rate 2 mm/min, extension direction NE315°–N135°E, and no syndeposition). Similar to the results of previous experiments [43–45], the initial stage of extension involves formation of a trunk boundary fault in the northern part of the model from the ductile and brittle base, forming a sinking rift zone (Figure 3(a)). Together with the antithetic secondary fault, they form a marginal graben. At this stage, all deformation is concentrated in the trunk boundary fault and the antithetic faults. Further stable extension promotes

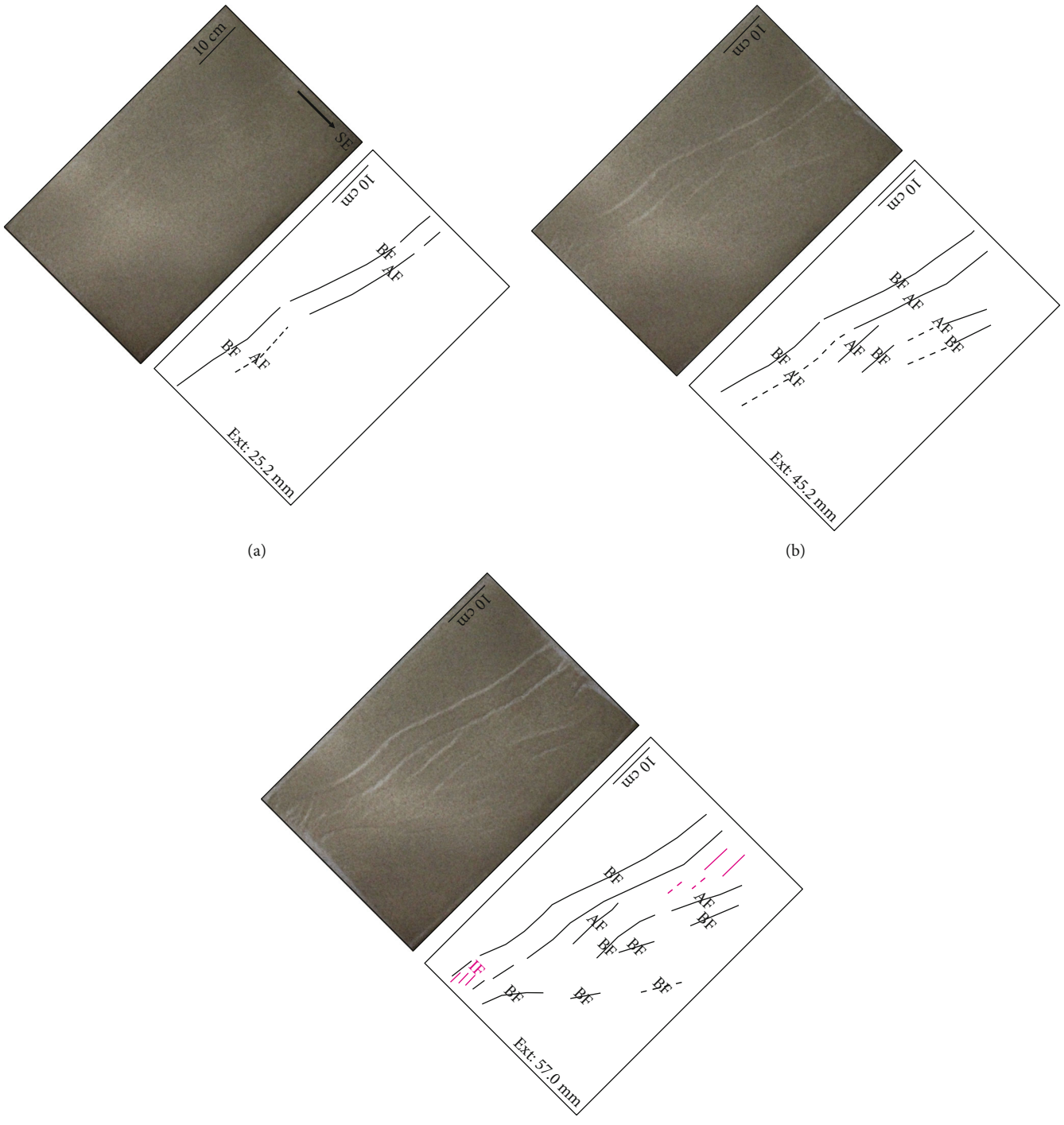

Figure 3: Continued.

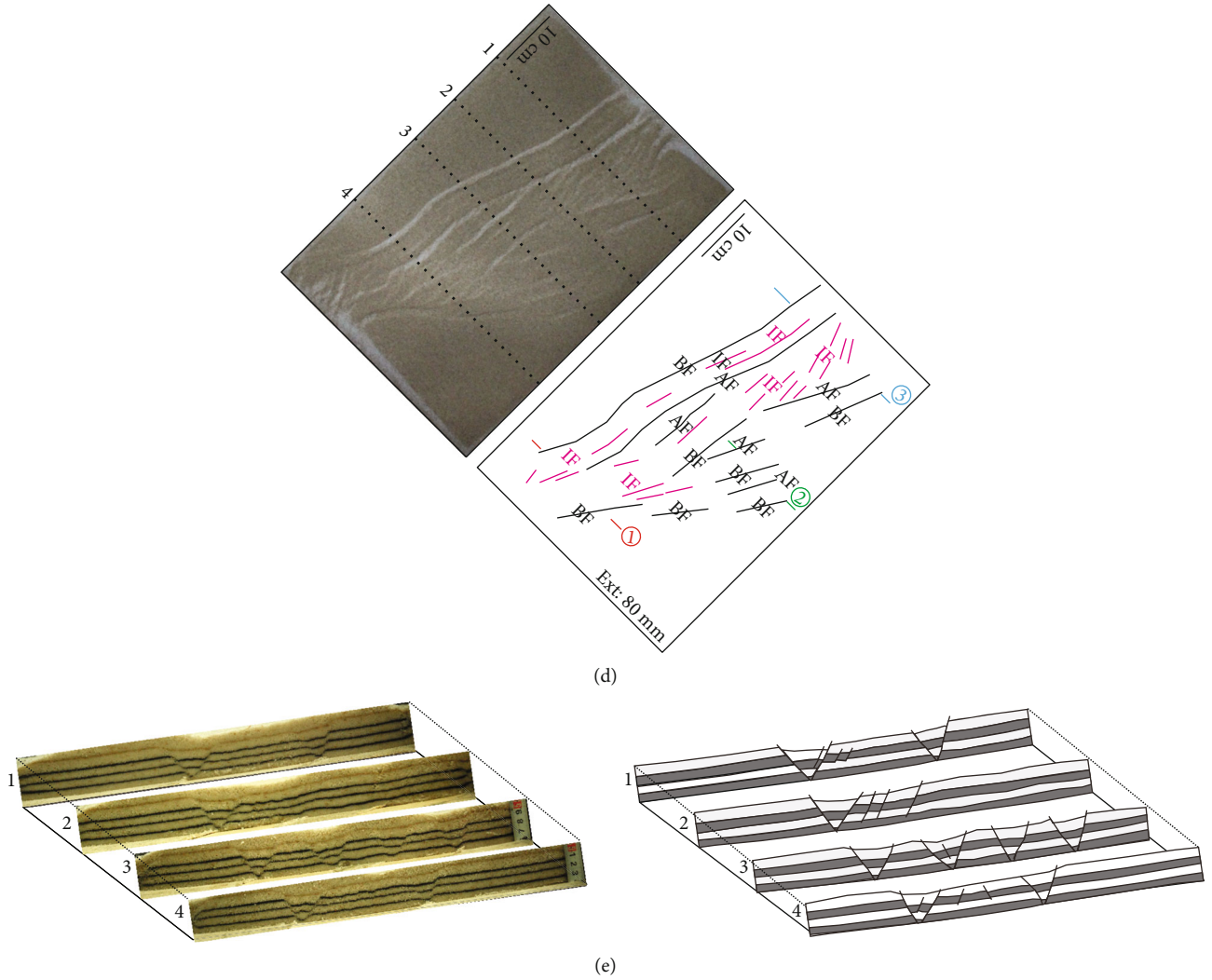

Figure 3: Evolution and characteristics of deformation in reference model 1. (a–d) Top-view photos (left panels) and schematic line-drawings of structures (right panels), illustrating boundary faults (BF), antithetic faults (AF), and internal faults (IF). (e) Vertical cross sections corresponding to locations in (d).

a change in the deformation pattern with extension of 57 mm (Figure 3(c)). The second master fault is formed at the boundary between the ductile base and the brittle base of the central horst zone, and the antithetic faults formed in the south of the model constitutes the second larger marginal graben, which undergoes further extension (Figures 3(c) and 3(d)) in the central horst zone to form a large number of secondary faults (the critical extension of the secondary fault when it first appears is determined by observing deformation of the model surface) [43–45]. Conversely, activity on the trunk boundary faults is reduced, eventually forming a structure in which the graben is arranged separately under steep boundary fault control. The final section clearly shows that four narrow grabens are juxtaposed in the center (Figure 3(e), slice 3). Close to the sides of the baffle, and these become two narrow grabens; thus, the closer to the baffle sides, the larger the interval between the grabens (Figure 3(e), slices 2, 4, and 5).

4.2. Effect of Extension Rate (Model 2). Model 2 has an extension rate of 4.0 mm/min, which is twice that of the reference model. The evolution of deformation still involves the initial boundary fault formation stage and the internal secondary fault formation and movement stage. As shown in Figure 4, the formation and movement of internal secondary faults occur when the amount of extension is 48 mm. This indicates that the rate of extension determines the amount of extension required for the evolution of internal secondary faults; a higher rate of extension leads to more rapid formation of internal secondary faults in the rift basin, thus requiring less amount of extension (Figure 5). However, the extension rate has little effect on the evolution of rift zone width (widest value in the vertical extension direction); all of them start at 20 mm extension and exhibit a positive correlation (Figure 6). The final cross section shows that the rifting system, in which the compound complex graben developed by a broad internal domino fault under the

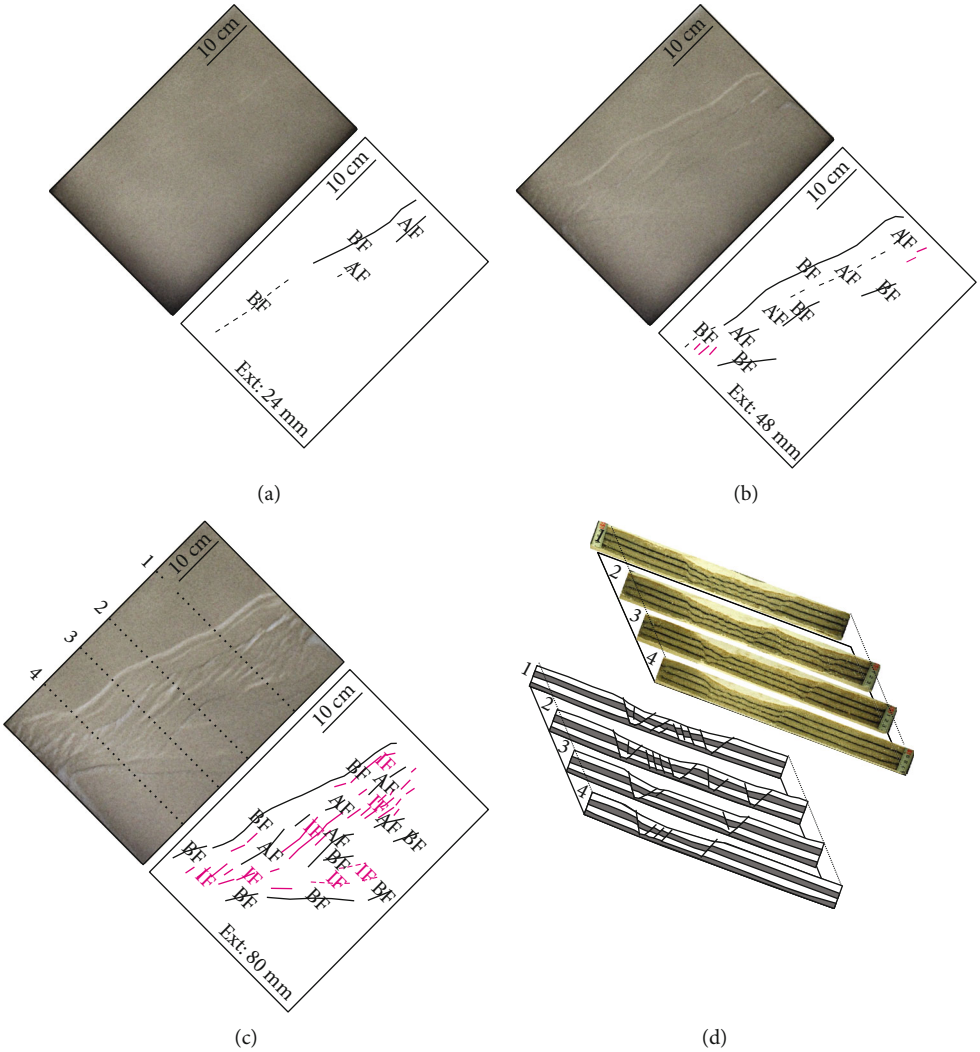

Figure 4: Evolution and characteristics of deformation in model 2, with a higher extension rate. (a–c) Top-view photos (left panels) and schematic line-drawings of structures (right panels), illustrating boundary faults (BF), antithetic faults (AF), and internal faults (IF). (d) Vertical cross sections corresponding to locations in (c).

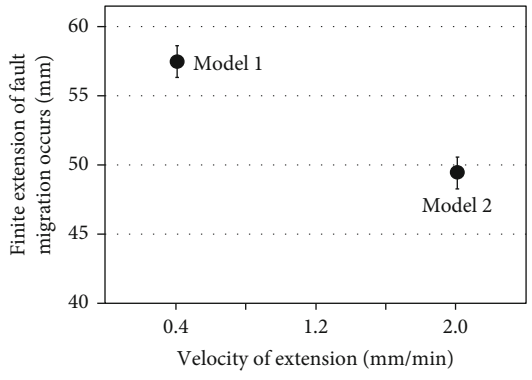

Figure 5: Summary of series 2 experiments (variable extension rate) illustrated as plots of the bulk extension corresponding to the first appearance of internal faults as a function of extension rate.

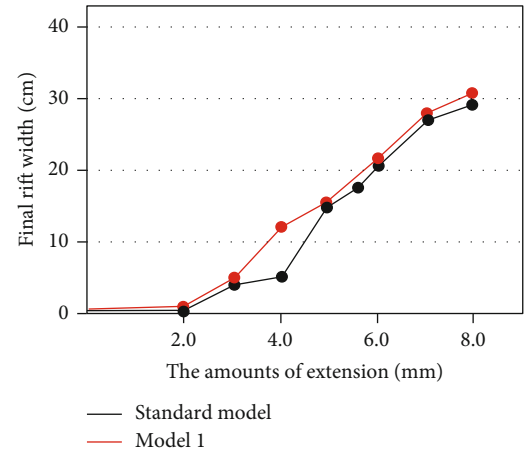

Figure 6: Final rift segment width as a function of extension, measured from the model surface views in Figures 4 and 5.

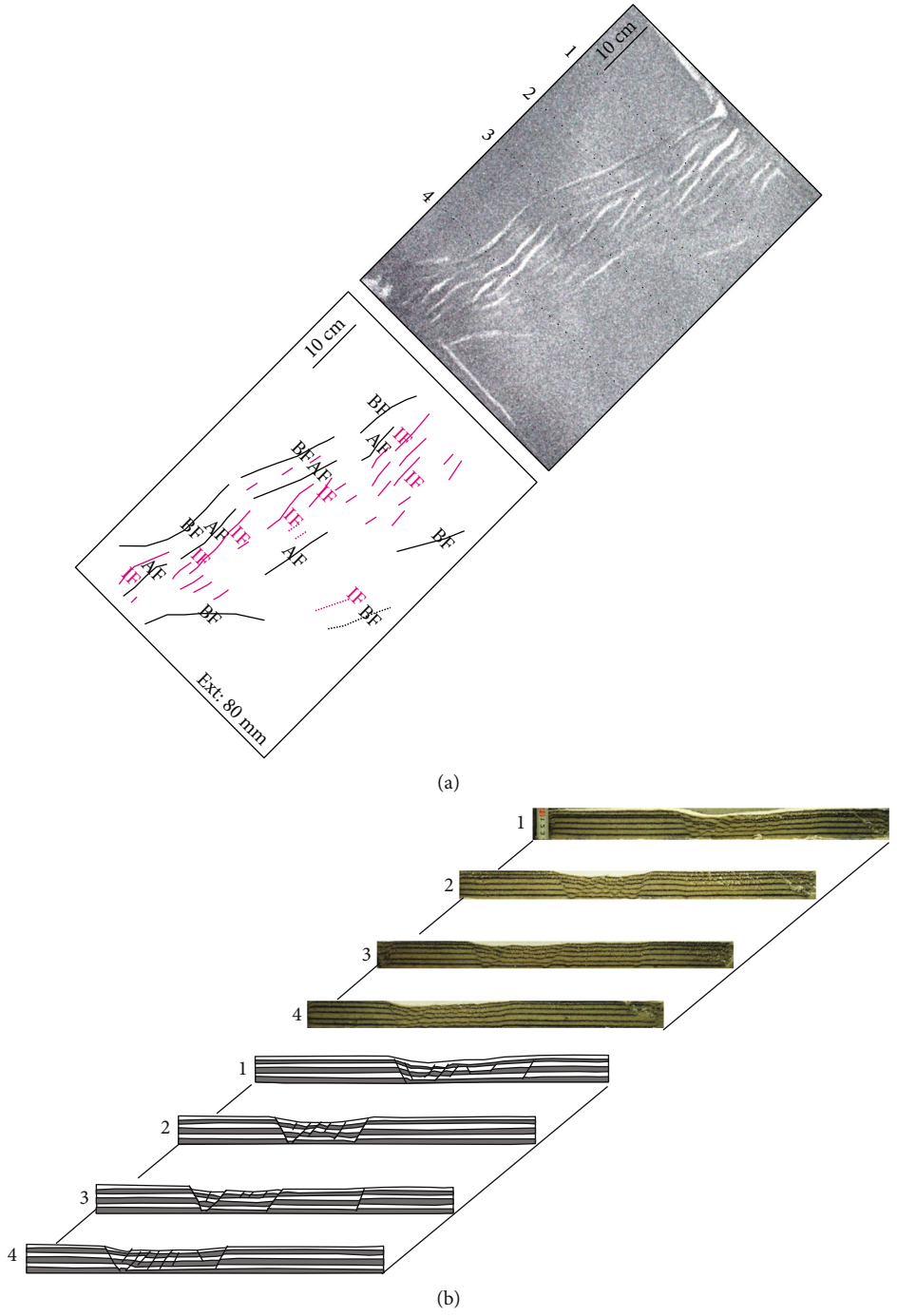

Figure 7: Evolution and characteristics of deformation in model 3, with thicker strata. (a) Top-view photo (upper panel) and schematic line-drawing of structures (lower panel), illustrating boundary faults (BF), antithetic faults (BF), and internal faults (IF). (b) Vertical cross sections corresponding to locations in (a).

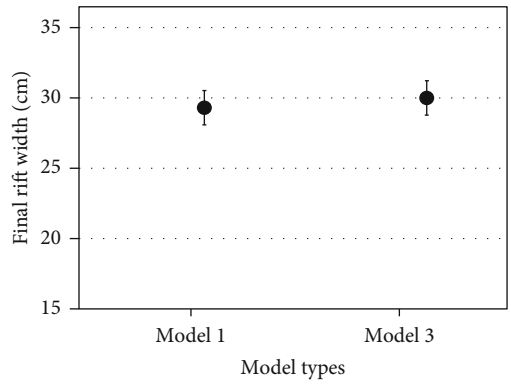

Figure 8: Final rift segment width as a function of extension, measured from the model surface.

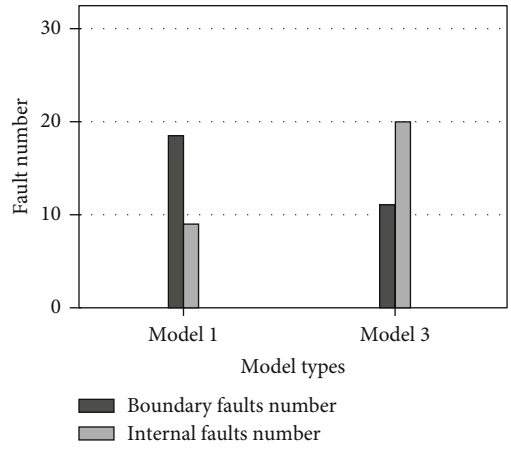

Figure 9: Number of faults in the reference model and model 3, where the number of faults is the sum of sections 1–4.

control of a trunk boundary fault and the simple graben are arranged separately, differs between models 1 and 2. That is, model 2 has more secondary faults for the same amount of extension (80 mm) (Figures 3(d) and 4(c)).

4.3. Effect of Syndeposition (Model 3). The evolution of deformation shown by model 3 is similar to that of the reference model; both exhibit complex rifting with internal secondary faults under the control of the master fault (Figure 7). Model 3 has a rift (30 cm) that is 2 cm wider after extension of 8 cm than the rift of the reference model (28 cm) (Figure 8). The deformation pattern observed in the cross section of model 3 is also similar to the reference model (Figure 7), but the number of internal faults (quantified by the total number of faults in the four sections) is 12 for the trunk boundary fault and 20 for the secondary fault. The reference model therefore has more master faults (18) and fewer secondary faults (9) (Figure 9), as well as fewer total faults. The experimental results show that syndeposition is equivalent to the thickness of the overlying brittle layer gradually increasing to the thickness of the reference model brittle layer and the strength of the overlying brittle

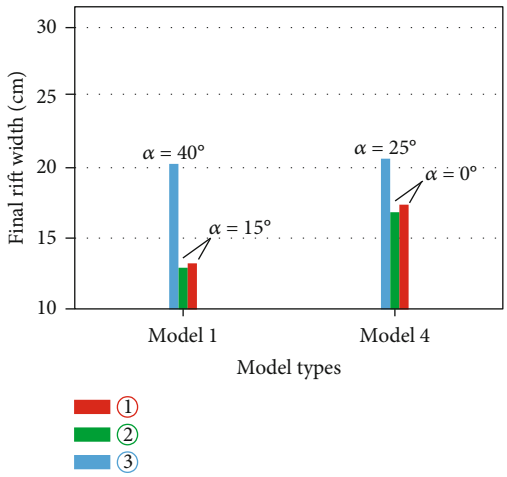

Figure 10: Relationship between different inclination angles and rifting width.

layer increasing to that of the reference model brittle layer. In this case, the width of the rift is greater, the number of trunk boundary faults is reduced, and the number of secondary faults is increased.

4.4. Effect of Extension Direction (Model 4). Model 4 exhibits a wider rift (35 cm) at 8 cm of extension, which is 7 cm wider than that of the reference model (28 cm). The rifting width of the three different cross sections is negatively correlated with the angle of extension obliquity (Figure 10). The dominant strike of the secondary fault of cross sections 1 and 2 of the model 4 is N62 E, which differs by 8 from the dominant strike (N70 E) of the reference model. The dominant strike of the secondary fault of cross-section 3 is N58 E, 15 of the dominant strike (N43 E) of the reference model (Figure 11). The experimental results show that extension obliquity at different angles controls the width of rifting and the strike of the internal secondary fault. The larger the inclination angle of oblique rifting, the wider the rift. The fault strike near the ductile rifting boundary is controlled by this oblique angle, which is approximately parallel to the strike of the master fault. The strike of the secondary fault inside the rift is predominantly controlled by the extension direction, which is almost perpendicular to the extension direction.

5. Discussion

5.1. Major Controlling Factors of Tectonic Deformation. The rate of extension of the lithosphere affects the tectonic evolution of rift basins ([45–47] for reviews). Our physical simulation results show that different extension rates control the amount of extension required for secondary fault appearance, in that a high extension rate corresponds to more rapid movement of the internal deformation in the rift basin. This is similar to the results of a physical simulation experiment conducted by Corti et al. [45]. We use retractable rubber instead of different viscosity silica gels in the base ductile

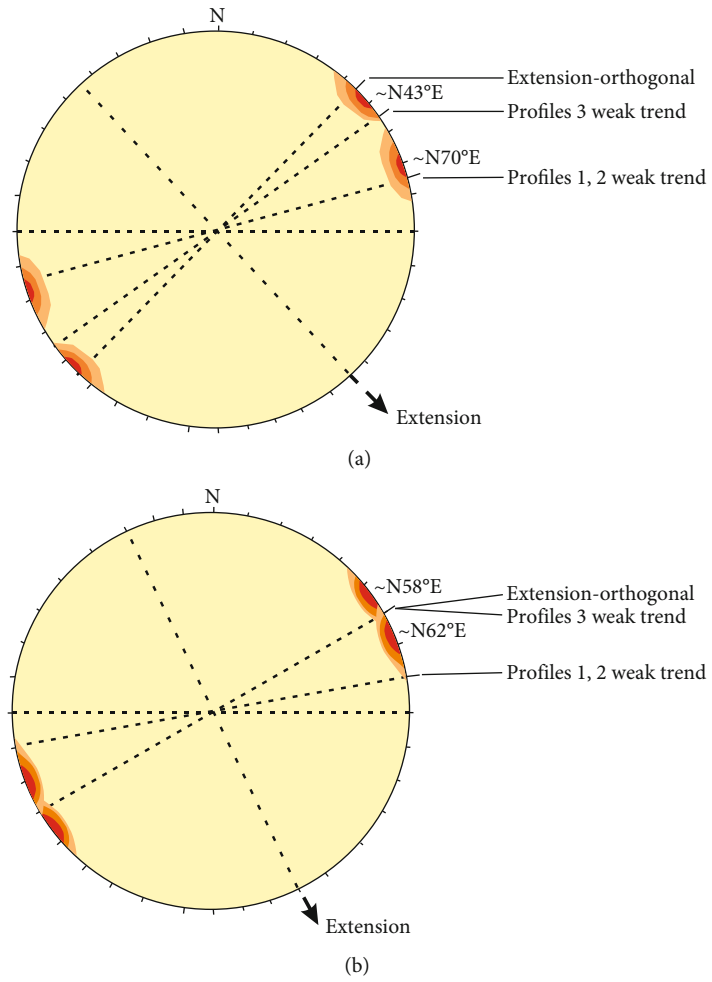

Figure 11: Rift zone fault dominant strike orientation map for the reference model and model 4.

layer [44, 45]. This may explain why our experiments exhibited more rapid deformation evolution. Due to the heterogeneity of extension rate and amount in different areas of the Erlian Basin [48], our physical simulation results show that, even if the extension rate and magnitude are small, it will lead to differences in rifting width and development of secondary faults (Figures 3 and 4).

The syndeposition is equivalent to increasing the thickness of the upper layer, thereby increasing the strength of the overlying brittle layer. An increase in the thickness of the overlying brittle layer (and thus strength of the brittle layer) inhibits the formation of axial faults [45]. This is the same as our research.

The direction of extension (equivalent to changing the angle of the oblique rift) is the main factor controlling the pattern of the rift structure [19, 21, 23, 27, 49]. Experimental results show that positive rifting forms a narrow positive rift zone dominated by normal faults with steep dip angles. Oblique rifting forms a broad oblique rifting zone dominated by "domino-type" faults. The larger the angle of rifting, the more developed the "domino-type" fault (Figures 4 and 12), which is similar to the experimental results of previous physical models [23, 50]. The larger the oblique angle of rifting (angle between the direction of extension and the normal direction of the rift strike), the more rapid the evolution of internal secondary faults [43].

5.2. Comparison with Nature. The Mesozoic rifting basin of Erlian in northeast China has the typical features of a continental rifting basin. Since the early Cretaceous, it has experienced a long period of intracontinental extensional rifting, recording the long-term extension process from early rifting to late depression. The Mesozoic rift zone is controlled by the early preexisting structural style of the basement lithosphere comprising; (1) the weak deformation zone of the basement formed by Paleozoic magmatic rock or the anticlinorium uplift zone, whose core is the Lower Paleozoic and (2) the strong deformation zone of the basement formed by the fold thrust belt or the synclinorium, whose core is the Carboniferous-Permian, and Erlian-Hegenshan melange belt and the Solon Obo-Xar Moron suture zone. In particular, the weak and strong basement boundary forms a number of trunk boundary faults that control the rift basin group. Continued extension and thinning of the lithosphere

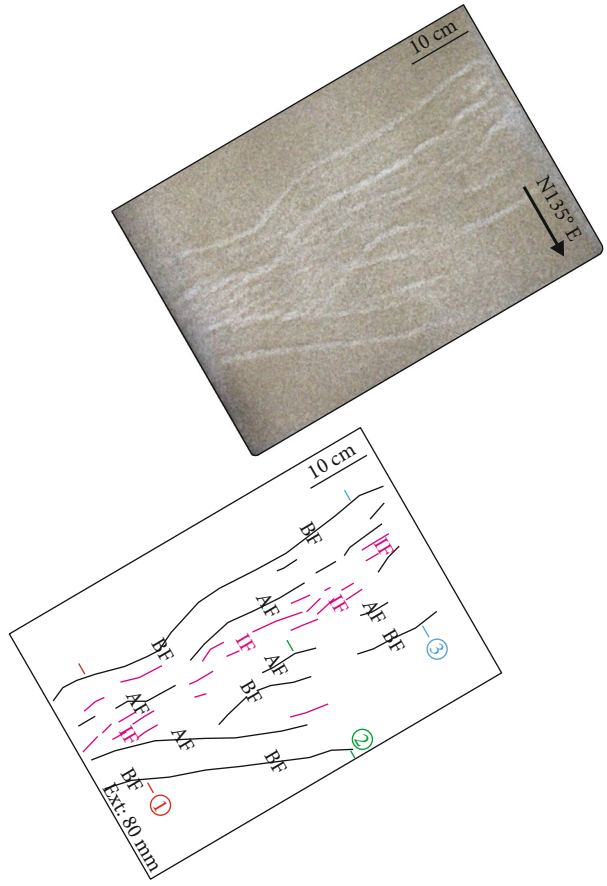

Figure 12: Evolution and characteristics of deformation in model 4, with a different extension direction. (a) Top-view photo (upper panel) and schematic line-drawing of structures (lower panel), illustrating boundary faults (BF), antithetic faults (AF), and internal faults (IF).

lead to central rifting, accompanied by the formation of a central secondary fault and cessation of the trunk boundary fault. The internal secondary fault of the rift formed in the early Cretaceous, and the central internal secondary fault formed later. Seismic data show that the rift obliquity of the secondary rift in the Erlian Basin is characterized by small inclinational angles (the angle between the extension direction and the axis of the rifting) in the north and central regions and large inclinational angles in the west and south. This indicates that trunk boundary fault activity and evolution of the internal secondary fault along the axial direction are strictly controlled by the thickness of the brittle and ductile layer (the increase in the thickness of the brittle layer is equivalent to the syndeposition) and the obliquity of rifting. Specifically, the narrow weak zone and the small angle of obliquity in the central part of the Erlian Basin make the boundary fault more active, and the central secondary fault is formed later.

Compared with the actual structural features of the Erlian Basin, except for the poor similarity of model 3, all models show good similarity in the deformation patterns (Figure 13). These models reproduce the overall structural pattern of the "5 depressions, 3 uplifts" in the basin: (1) Chuanjing Sag of NEE and EW faults, (2) Wulanchabu Sag and Sunite Sag of NNE and NE faults with longer extension, (3) Sunite Sag of NNE and near NS faults with large intervals between faults, and (4) Tenggeer Sag of NE and NNE faults; relatively underdeveloped faults in this area may be due to the depression being close to the direction of extension and the rubber being less stretched.

Although the extension direction of model 3 is only 15° different from that of other models, it exhibits very low similarity in its structural pattern. The strike of internally developed faults is NEE and EW (Figure 11), which is similar to the dominant orientation of fault strike developed in Chuanjing Sag and Tenggeer Sag. Other factors such as fault combination and extension length display low similarity. In addition, when the extension is small, the deformation pattern of model 3 is not as good as that of the actual structure of Erlian Basin (Figure 13), which indicates that the magnitude of extension is not the cause of the lack of similarity.

Figure 11 reflects that the dominant orientation of the secondary fault strike of the standard model is similar to that of the actual master fault of Erlian Basin. However, the dominant orientation of the master fault of model 3 is less similar to the actual situation, which also indicates that inconsistency of the fault strike inside the rift basin and the complex kinematic mechanism is not necessarily inevitable. The fault strike inside the basin far from the boundary is mainly controlled by the direction of structural extension [51]. By

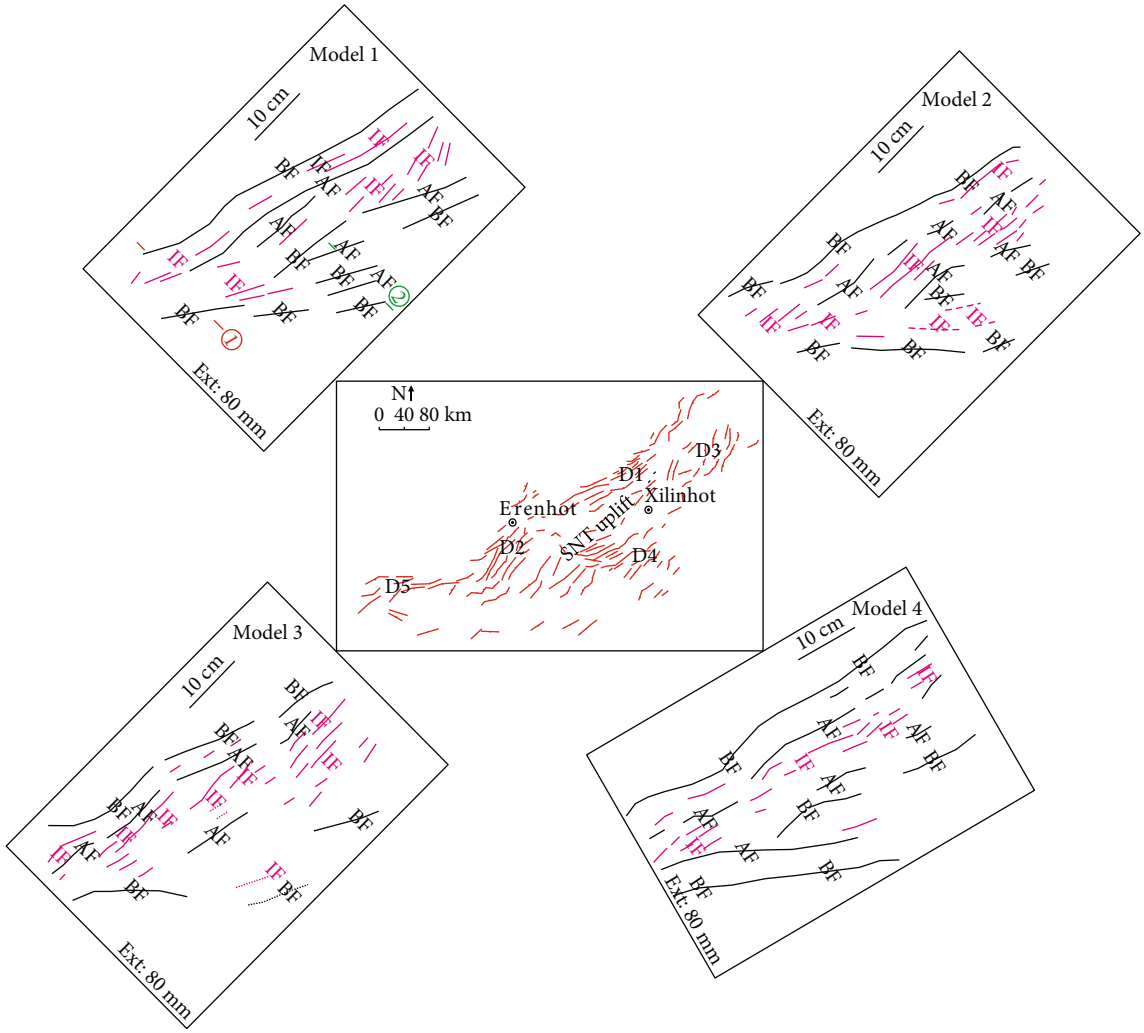

Figure 13: Comparison between experimental models and the actual geologic structure of Erlian Basin.

comparing the physical simulation experiments of different extension directions, we propose that Erlian Basin was formed by extension in the direction N315°E–N135°E. Strike-slip deformation of the boundary faults in the western and eastern of the basin is therefore the result of uniform N315°–135E° extension and different angles of the basement ductile zone ($\alpha = 0°$, 10°), which plays a role in lateral conversion. We suggest that the "N315°E–N135°E direction extension mode" provides a good kinematic explanation for the formation of the Erlian Basin and similar rift basins in northeastern China.

6. Conclusions

We applied the physical simulation method to study the effects of extension rate, extension direction, and syndeposition on the Mesozoic tectonic deformation of the Erlian Basin and obtained the following conclusions:

(1) The results of extension models with different extension rates and syndeposition are similar to the actual geological structure of the basin, but there are differences in the deformation evolution process and deformation patterns. An increase of the extension rate promotes earlier appearance of secondary faults inside the rift and increases the width of the rift

(2) Syndeposition is equivalent to increasing the strength of the overlying brittle layer, which promotes the development of internal secondary faults, favors a wider rift, and conversely suppresses the development of master faults

(3) The similarity between the experimental results of the N330°E–N150°E extension model and the actual geologic structure is poor. However, the experimental results show that the magnitude of extension is not the cause of the lack of similarity. When the angle of rifting is small, a narrow positive rifting zone is formed. When the angle is large, a gentle oblique rifting zone is formed. Extension direction controls faults inside the rift zone far from the extension boundary. Good similarities between the

different extension models and the actual geologic structure indicate that the Erlian Basin was formed by extension in the southeast direction. The physical simulation experimental model designed in this study can provide some reference for the research on the tectonic evolution of similar basins

Data Availability

The data used to support the findings of this study are included within the article.

Conflicts of Interest

The authors declare that they have no conflicts of interest.

Acknowledgments

This work was supported by the China National 973 Project (2015CB453000) and China Geological Survey Project (12120115009801).

References

[1] S. T. Li, S. G. Yang, C. L. Wu et al., "Late Mesozoic rift in Northeast China and Northeast Asian Fault Basin," *Science in China Series B Chemistry*, vol. 2, pp. 185–195, 1987.

[2] S. T. Li, *Evolution of the Mesozoic and Cenozoic Basins in the Eastern and Adjacent Areas of China and the Geodynamic Background*, China University of Geosciences, Wuhan, 1997.

[3] Q. R. Meng, J. M. Hu, X. J. Yuan, and J. Q. Jin, "Structure evolution and origin of Late Mesozoic extensional basins in the China-Mongolia border region," *Geological Bulletin of China*, vol. 21, pp. 224–231, 2002.

[4] Q. R. Meng, "What drove late Mesozoic extension of the northern China-Mongolia tract," *Tectonophysics*, vol. 369, no. 3-4, pp. 155–174, 2003.

[5] J. Y. Ren, S. T. Li, and G. H. Jiao, "Extensional tectonic system of Erlian fault basin group and its deep background," *Earth Science*, vol. 23, pp. 567–572, 1998.

[6] J. A. Shao, *Northeast China Terrain and Northeast Asian Continent Evolution*, Seismological Press, 1995.

[7] T. T. Yan, Y. B. Yao, and D. M. Liu, "Critical tectonic events and their geological controls on gas generation, migration, and accumulation in the Weibei coalbed methane field, southeast Ordos basin," *Journal of Natural Gas Science and Engineering*, vol. 27, pp. 1367–1380, 2015.

[8] T. T. Yan, S. He, Y. Bai et al., "A study on the heterogeneity characteristics of geological controls on coalbed methane accumulation in Gujiao coalbed methane field, Xishan Coalfield, China," *Geofluids*, vol. 3, 20 pages, 2021.

[9] A. C. Xiao, S. F. Yang, and H. L. Chen, "Geodynamic background on formation of Erlian basin," *Oil and Gas Geology*, vol. 22, pp. 137–140, 2001.

[10] Y. Q. Zhang, Y. Zhao, S. W. Dong, and N. Yang, "Tectonic evolution stages of the Early Cretaceous rift basins in Eastern China and adjacent areas and their geodynamic background," *Geoscience Frontiers*, vol. 11, pp. 123–133, 2004.

[11] C. L. Zhao, "Formation mechanism of reservoir space and oil possibility of volcanic reservoirs," *Geological Review*, vol. 42, pp. 37–43, 1996.

[12] Z. Y. Tian, P. Han, and K. D. Xu, "The Mesozoic-Cenozoic East China rift system," *Tectonophysics*, vol. 208, no. 1-3, pp. 341–363, 1992.

[13] Z. Y. Tian and B. Q. Shi, "Geological features and petroleum reservoir formation in Meso-Cenozoic sedimentary basins in China," *Geotectonica et Metallogenia*, vol. 26, pp. 1–5, 2002.

[14] Y. Q. Cui, X. H. Liu, Z. H. Sun, H. Yao, and C. Y. Han, "The deep physical geographic characteristics and Neopaleozoic geological structural exploration of Erlian basin, Inner Mongolia," *Geological Bulletin of China*, vol. 30, pp. 235–242, 2011.

[15] X. P. Li, S. H. Zhang, L. B. Li et al., "Coupling of faulted sags to basement in the Early Cretaceous Erlian Basin," *Chinese Journal of Geology*, vol. 50, pp. 88–99, 2015.

[16] J. F. Qi, X. Z. Zhao, X. P. Li et al., "The distribution of Early Cretaceous faulted-sags and their relationship with basement structure within Erlian Basin," *Geoscience Frontiers*, vol. 22, pp. 118–128, 2015.

[17] Z. Cai, Q. Huang, B. Xia, and J. Xiang, "Differences in shale gas exploration prospects of the upper Yangtze Platform and the lower Yangtze Platform: insights from computer modelling of tectonic development," *Journal of Natural Gas Science and Engineering*, vol. 36, pp. 42–53, 2016.

[18] L. Wang, S. Wang, R. Zhang et al., "Review of multi-scale and multi-physical simulation technologies for shale and tight gas reservoirs," *Journal of Natural Gas Science and Engineering*, vol. 37, pp. 560–578, 2017.

[19] M. Bonini, T. Souriot, M. Boccaletti, and J. P. Brun, "Successive orthogonal and oblique extension episodes in a rift zone: laboratory experiments with application to the Ethiopian rift," *Tectonics*, vol. 16, no. 2, pp. 347–362, 1997.

[20] Y. Mart and O. Dauteuil, "Analogue experiments of propagation of oblique rifts," *Tectonophysics*, vol. 316, no. 1-2, pp. 121–132, 2000.

[21] K. R. McClay and M. J. White, "Analogue modelling of orthogonal and oblique rifting," *Marine and Petroleum Geology*, vol. 12, no. 2, pp. 137–151, 1995.

[22] J. X. Zhou and J. S. Zhou, "Cenozoic tectonic deformation mechanism in the Bohai Bay Basin: physical simulation and discussion," *Science China Earth Sciences*, vol. 36, pp. 507–519, 2006.

[23] F. Zwaan, G. Schreurs, J. Naliboff, and S. J. H. Buiter, "Insights into the effects of oblique extension on continental rift interaction from 3D analogue and numerical models," *Tectonophysics*, vol. 693, pp. 239–260, 2016.

[24] A. Chemenda, J. Déverchère, and E. Calais, "Three-dimensional laboratory modelling of rifting: application to the Baikal Rift," *Russia. Tectonophysics*, vol. 356, no. 4, pp. 253–273, 2002.

[25] K. McClay and T. Dooley, "Analogue models of pull-apart basins," *Geology*, vol. 23, no. 8, pp. 711–714, 1995.

[26] D. Paul and S. Mitra, "Experimental models of transfer zones in rift systems," *AAPG Bulletin*, vol. 97, no. 5, pp. 759–780, 2013.

[27] J. Autin, N. Bellahsen, S. Leroy, L. Husson, M. O. Beslier, and E. Acremont, "The role of structural inheritance in oblique rifting: insights from analogue models and application to the Gulf of Aden," *Tectonophysics*, vol. 607, pp. 51–64, 2013.

[28] T. Dooley and K. McClay, "Analog modeling of pull-apart basins," *AAPG Bulletin*, vol. 81, pp. 1804–1826, 1997.

[29] H. M. Tong, L. J. Meng, D. S. Cai, Y. P. Wu, X. S. Li, and M. Q. Liu, "Fault formation and evolution in rift basins-sandbox

modeling and cognition," *ACTA Geol Sin*, vol. 6, pp. 759–774, 2009.

[30] X. Z. Zhao, F. M. Jin, J. F. Qi et al., "The structural types and petroleum geological significance of Early Cretaceous complex faulted sag in Erlian Basin," *Natural Gas Geoscience*, vol. 26, pp. 1289–1298, 2015.

[31] J. B. Zhou, X. Z. Zhang, Z. H. Ma et al., "Tectonic framework and basin evolution in Northeast China," *Oil and Gas Geology*, vol. 30, pp. 530–538, 2009.

[32] X. Z. Zhang, B. J. Yang, F. Y. Wu, and G. X. Liu, "The lithosphere structure in the Hingmong-Jihei (Hinggan-Mongolia-Jilin-Heilongjiang) region, northeastern China," *Geologyin-China*, vol. 33, pp. 816–823, 2006.

[33] G. Corti, G. Ranalli, and D. Sokoutis, "Quantitative modelling of geological processes preface," *Tectonophysics*, vol. 484, no. 1-4, pp. 1–3, 2010.

[34] K. McClay and M. Bonora, "Analog models of restraining stepovers in strike-slip fault systems," *AAPG Bulletin*, vol. 85, no. 2, pp. 233–260, 2001.

[35] H. M. Tong, D. S. Cai, Y. P. Wu, X. G. Li, X. S. Li, and L. J. Meng, "Determination of pre-existing tectonic activity in non-uniform deformation," *Science China Earth Sciences*, vol. 41, pp. 158–168, 2011.

[36] J. X. Zhou, F. Y. Xu, C. G. Weia, G. Li, F. S. Yua, and H. M. Tong, "Shortening of analogue models with contractive substrata: insights into the origin of purely landward-vergent thrusting wedge along the Cascadia subduction zone and the deformation evolution of Himalayan-Tibetan orogen," *Earth and Planetary Science Letters*, vol. 260, no. 1-2, pp. 313–327, 2007.

[37] J. X. Zhou, B. Zhang, and Q. Xu, "Effects of lateral friction on the structural evolution of fold-andthrust belts: insights from sandbox experiments with implications for the origin of landward-vergent thrust wedges in Cascadia," *Geological Society of America Bulletin*, vol. 128, no. 3-4, pp. 669–683, 2016.

[38] F. Nilfouroushan, R. Pysklywec, and A. Cruden, "Sensitivity analysis of numerical scaled models of fold-and-thrust belts to granular material cohesion variation and comparison with analog experiments," *Tectonophysics*, vol. 526-529, pp. 196–206, 2012.

[39] H. Ramberg, *Gravity, Deformation and the Earth's Crust*, Academic Press, London, 1981.

[40] M. Bonini, F. Sani, and B. Antonielli, "Basin inversion and contractional reactivation of inherited normal faults: a review based on previous and new experimental models," *Tectonophysics*, vol. 522, pp. 55–88, 2012.

[41] G. Mulugeta, "Squeeze box in the centrifuge," *Tectonophysics*, vol. 148, no. 3-4, pp. 323–335, 1988.

[42] G. Corti, "Centrifuge modelling of the influence of crustal fabrics on the development of transfer zones: insights into the mechanics of continental rifting architecture," *Tectonophysics*, vol. 384, no. 1-4, pp. 191–208, 2004.

[43] A. Agostini, G. Corti, A. Zeoli, and G. Mulugeta, "Evolution, pattern and partitioning of deformation during oblique continental rifting: inferences from lithospheric-scale centrifuge models," *Geochemistry, Geophysics, Geosystems*, vol. 10, no. 11, pp. 1–23, 2009.

[44] G. Corti, "Control of rift obliquity on the evolution and segmentation of the main Ethiopian rift," *Nature Geoscience*, vol. 1, no. 4, pp. 258–262, 2008.

[45] G. Corti, G. Ranalli, A. Agostini, and D. Sokoutis, "Inward migration of faulting during continental rifting: effects of pre-existing lithospheric structure and extension rate," *Tectonophysics*, vol. 594, pp. 137–148, 2013.

[46] J. P. Brun, "Narrow rifts versus wide rifts: inferences for the mechanics of rifting from laboratory experiments," *Philosophical Transactions of the Royal Society of London. Series A: Mathematical, Physical and Engineering Sciences*, vol. 357, no. 1753, pp. 695–712, 1999.

[47] L. Michon and O. Merle, "Mode of lithospheric extension: conceptual models from analogue modeling," *Tectonics*, vol. 22, no. 4, 2003.

[48] J. Y. Ren, K. Tamaki, S. T. Li, and Z. Junxia, "Late Mesozoic and Cenozoic rifting and its dynamic setting in Eastern China and adjacent areas," *Tectonophysics*, vol. 344, no. 3-4, pp. 175–205, 2002.

[49] L. Michon and D. Sokoutis, "Interaction between structural inheritance and extension direction during graben and depocentre formation: an experimental approach," *Tectonophysics*, vol. 409, no. 1-4, pp. 125–146, 2005.

[50] M. Philippon, E. Willingshofer, D. Sokoutis, M. Bonini, and S. Cloetingh, "Slip re-orientation in oblique rifts," *Geology*, vol. 43, no. 2, pp. 147–150, 2015.

[51] J. X. Zhou and J. F. Qi, "Sandbox experimental modeling of oblique extensional rifting with kink boundary," *Journal of Earth ScienceChina*, vol. 24, pp. 630–634, 1999.